Title

Hippocampal CA3 inhibitory neurons receive extensive noncanonical synaptic inputs from CA1 and subicular complex.

Journal

The Journal of Comparative Neurology, 531(13)

Authors

Lin, Xiaoxiao
Cyrus, Neeyaz
Avila, Brenda
et al.

Publication Date

2023-09-01

DOI

10.1002/cne.25510

Peer reviewed

HHS Public Access

Author manuscript

J Comp Neurol. Author manuscript; available in PMC 2024 September 01.

Published in final edited form as:

J Comp Neurol. 2023 September ; 531(13): 1333–1347. doi:10.1002/cne.25510.

Hippocampal CA3 inhibitory neurons receive extensive noncanonical synaptic inputs from CA1 and subicular complex

Xiaoxiao Lin[a], **Neeyaz Cyrus**[a], **Brenda Avila**[a], **Todd C. Holmes**[b], **Xiangmin Xu**[a,1]

[a]Department Anatomy & Neurobiology, School of Medicine, University of California, Irvine, CA 92697

[b]Department Physiology & Biophysics, School of Medicine, University of California, Irvine, CA 92697

Abstract

Hippocampal CA3 is traditionally conceptualized as a brain region within a unidirectional feedforward trisynaptic pathway that links major hippocampal subregions. Recent genomic and viral tracing studies indicate that the anatomical connectivity of CA3 and the trisynaptic pathway is more complex than initially expected and suggests that there may be cell type specific input gradients throughout the 3-dimensional hippocampal structure. In several recent studies using multiple viral tracing approaches, we describe subdivisions of the subiculum complex and ventral hippocampal CA1 that show significant back projections to CA1 and CA3 excitatory neurons. These novel connections form “noncanonical” circuits that run in the opposite direction relative to the well characterized feedforward pathway. Diverse subtypes of GABAergic inhibitory neurons participate within the trisynaptic pathway. In the present study, we have applied monosynaptic retrograde viral tracing to examine noncanonical synaptic inputs from CA1 and subicular complex to the inhibitory neuron in hippocampal CA3. We quantitatively mapped synaptic inputs to CA3 inhibitory neurons to understand how they are connected within and beyond the hippocampus formation. Major brain regions that provide typical inputs to CA3 inhibitory neurons include the medial septum, the dentate gyrus, the entorhinal cortex and CA3. Noncanonical inputs from ventral CA1 and subicular complex to CA3 inhibitory neurons follow a proximodistal topographic gradient with regard to CA3 subregions. We find novel noncanonical circuit connections between inhibitory CA3 neurons and ventral CA1, subiculum complex and other brain regions. These results provide a new anatomical connectivity basis to further study the function of CA3 inhibitory neurons.

Graphical Abstract.

[1]Corresponding author: Dr. Xiangmin Xu, Department of Anatomy and Neurobiology, School of Medicine, University of California, Irvine, CA 92697-1275, xiangmix@uci.edu.

Author Contributions:

X.L., N.C., B.A. performed experiments and collected data. X.L., T.C.H. and X.X. analyzed the data, prepared the illustrations and wrote the manuscript with the help and input from other authors. X.X. oversaw the project.

Statement of conflict of interests

All authors disclose no conflict of interests for this work.

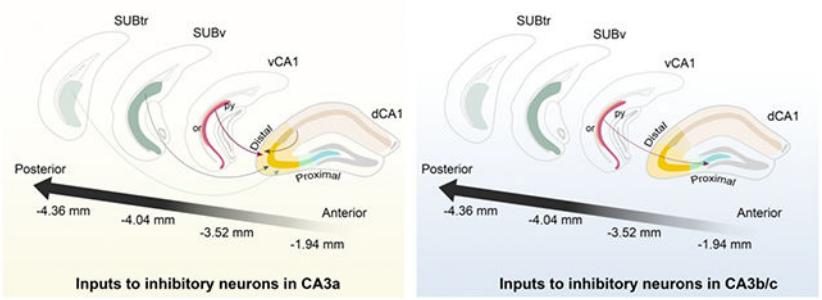

Lin et al., have applied monosynaptic retrograde viral tracing to examine both typical and non-canonical circuit inputs to CA3 inhibitory neurons in the mouse to understand how they are connected within and beyond the hippocampus formation. Noncanonical inputs from ventral CA1 and subicular complex to dorsal CA3 inhibitory neurons follow a proximodistal topographic gradient relative to CA3 subregions. This work provides a new anatomical connectivity basis to further study the function of CA3 inhibitory neurons.

Keywords

Hippocampal formation; subiculum; dorsal CA3; contralateral CA3; ventral CA1; circuit tracing; rabies virus; RRID:AB_2645298; RRID:AB_325403; RRID:IMSR_JAX:005359; RRID:IMSR_JAX:010802; RRID:AB_477652; RRID:AB_2307313; RRID:AB_2631173; RRID:AB_965456; RRID:AB_572270; RRID:AB_258806; BIOLOGICAL SCIENCES; Neuroscience

Introduction

Hippocampal CA3 plays a critical role in learning and memory consolidation. The anatomical connections of CA3 with the other subregions of the hippocampus have been studied by using conventional chemical tracing techniques (Cenquizca and Swanson, 2007; Dong *et al.*, 2009; Swanson and Cowan, 1977; Swanson *et al.*, 1981). These studies show that CA3 serves as a transitional region that transfers mossy fiber inputs from the dentate gyrus (DG) to CA1 in the trisynaptic model (Amaral and Witter, 1989; Andersen *et al.*, 1971; Ishizuka, 2008; Witter, 2007). Classically, excitatory information is transferred along the trisynaptic pathway in a feedforward direction to the major output region, the subiculum (SUB) (Andersen *et al.*, 1969; Steward, 1976; Witter *et al.*, 2017). However, recent genomic and viral tracing studies reveal that the anatomical connectivity of CA3 and the trisynaptic pathway shows further complexities (Dong *et al.*, 2009; Lin *et al.*, 2021; Sun *et al.*, 2019; Sun *et al.*, 2014; Thompson *et al.*, 2008; Xu *et al.*, 2016).

CA3 has been conceptualized as a homogenous network that supports autoassociative memory (Korol *et al.*, 1993; Marr, 1971). However, more recent genomic mapping studies reveal complexity and gene expression profiles divide the mouse hippocampal CA3 into 9 distinct subdomains along the proximodistal and septotemporal axes (Thompson *et al.*, 2008). Heterogeneities in anatomical connectivity and molecular expression along the proximodistal (transverse axis) mediate specific functions as shown by physiological

and behavioral experiments (Knierim and Neunuebel, 2016; Lee *et al.*, 2015; Lu *et al.*, 2015). Distal and proximal CA3 subregions correspond to pattern complexion and pattern separation, respectively (Lee *et al.*, 2004; Leutgeb *et al.*, 2004). Electrophysiological studies in brain slices or ex vivo hippocampal preparations show that hippocampal theta (8 Hz) network oscillations can flow "in reverse" from SUB to CA1 and CA3 to modulate spike timing and local network rhythms in these subregions (Jackson *et al.*, 2014). To better understand the anatomical basis of these "reverse oscillations," our group used multiple genetically modified viral tracers to identify a noncanonical SUB-backprojection to CA1 and CA3 excitatory neurons (Lin *et al.*, 2021; Sun *et al.*, 2014). Our results suggest that a projection from ventral CA1 (vCA1) excitatory to dorsal CA3 (dCA3) excitatory neurons may mediate the "reverse direction" theta oscillation along the septotemporal axis. Functionally, the vCA1 to dCA3 back-projection contributes to object-related memory, but not stress-related memory.

The hippocampus consists of ~90% excitatory neurons and also contains ~10% GABAergic inhibitory neurons (Freund and Buzsaki, 1996; Pelkey *et al.*, 2017). The trisynaptic pathway is modulated by GABAergic inhibitory neurons in both feedforward and feedback directions (Chamberland and Topolnik, 2012; Germroth *et al.*, 1989; Jaffe and Gutierrez, 2007; Lawrence and McBain, 2003; Misgeld and Frotscher, 1986; Wittner *et al.*, 2006). The CA3 subregions contain diverse subtypes of GABAergic inhibitory neurons that can be differentiated according to their chemical, physiological, morphological and synaptic connections (Acsady *et al.*, 1998; Klausberger and Somogyi, 2008; Lawrence and McBain, 2003). Based on earlier studies, CA3 inhibitory neurons are known to receive inputs from the medial septum (MS), the DG and the entorhinal cortex (EC) (Freund and Antal, 1988; Germroth *et al.*, 1989; Jaffe and Gutierrez, 2007; Melzer *et al.*, 2012). Medial septal GABAergic cells preferentially innervate axo-axonic GABAergic inhibitory neurons in CA3 (Joshi *et al.*, 2017; Salib *et al.*, 2019). Mossy fibers form four times more synaptic connections to CA3 inhibitory neurons relative to their inputs to excitatory neurons (Jaffe and Gutierrez, 2007). Str. lacunsom moleculare CA3 inhibitory neurons (Picard *et al.*) receive EC layer II inputs via perforant pathway (Germroth *et al.*, 1989; Melzer *et al.*, 2012). However, noncanonical circuit connections to CA3 inhibitory neurons have not been studied, and quantitative characterization of local and long-distance inputs (including noncanonical connections) to the subregions of CA3 inhibitory neurons needs to be determined.

In this study, we followed our previous CA3 excitatory neuron tracing studies (Lin *et al.*, 2021) to perform retrograde viral tracing of circuit inputs to CA3 inhibitory neurons in different dorsal CA3 locations (distal CA3, dCA3a; proximal CA3, dCA3b/c). We used a monosynaptic rabies virus tracing system (Lin *et al.*, 2021; Sun *et al.*, 2019; Sun *et al.*, 2014; Sun *et al.*, 2018; Wickersham *et al.*, 2007), and quantitatively mapped the whole-brain-wide inputs to dorsal CA3 (dCA3) inhibitory neurons along proximodistal (transverse) and septotemporal axes. We determined the anatomical connectivity of canonical and noncanonical connections to hippocampal CA3 inhibitory neurons. The updated anatomical map will allow us to better study the functions of hippocampal CA3 inhibitory neurons by consideration of the noncanonical circuit connections.

Materials and Methods

Animals

All experiments were performed in accordance with the National Institutes of Health Animal Care and Use Guidelines and were approved by the Institutional Animal Care and Use Committee (IACUC) and the Institutional Biosafety Committee of the University of California, Irvine (IACUC protocol number: AUP-20-002). For viral circuit tracing experiments, GAD2-Cre (JAX stock #010802) and Camk2α-Cre (T29) (JAX stock # 005359) mice were used to map inputs to CA3 inhibitory neurons and excitatory neurons, respectively. For more information, see the text in S1 table.

Viral injections

Detailed procedures for viral injection have been described in our earlier work (Sun *et al.*, 2014). Mice were anesthetized under 1.5% isoflurane for 10 minutes with a 0.8 L/min oxygen flow rate using an isoflurane tabletop unit (HME109, Highland Medical Equipment, Temecula, CA, USA). Mice were transferred to a rodent stereotaxic frame (Leica Angle Two for mouse, Leica BiosystemsInc., Buffalo Grove, IL, USA), and were anesthetized with 1% isoflurane. To reflect the skin, a small incision was made in the head, and the skull was exposed to show the landmarks of bregma and lambda. A 3-axis micromanipulator guided by a digital atlas was used to calculate the injection site coordinates relative to the bregma and lambda. The virus was delivered to the target region.

Two ways of viral tracer delivery were utilized: picospritzer pressure injection and iontophoretic current injection. Pressure injection infects a large number of cells in the injection point, but iontophoretic current injection restricts the size of infected areas within a small target region. Either injection method showed no biased inputs from different brain regions. The procedure for pressure injection included drilling a small hole in the skull, above the injection site, which exposes the pia surface. The virus was then loaded into a glass pipette (tip diameter, approximately 10–20 μm) and lowered into the brain at targeted coordinates. A picospritzer (Parker Hannifin, Hollis, NH, USA) was used to pulse the virus into the brain at a rate of 20 to 30 nL/min with a 10-ms pulse duration. The procedure for iontophoresis included delivering the virus with a positive 3-μA current in a cycle of 7 seconds “on” and 7 seconds “off” for a duration of 10 minutes. To prevent backflow of the virus, the injection pipette remained in the brain for 5 minutes after completion of the injection. Once the injection pipette was withdrawn, the mouse was removed from the stereotaxic frame, and tissue adhesives (3M Vetbond, St. Paul, Minnesota, USA) were used to close the incision. Mice were then given a Carprofen injection and taken back to their home cages for recovery.

Adeno-associated virus (AAV) and rabies virus

To map and quantitatively analyze the input connection strengths of inhibitory or excitatory CA3 cells, we used genetically modified rabies virus and the mouse lines expressing Cre-recombinase. The rabies infections were restricted to specific localized CA3 subregions without leaks to CA1. We achieved this using genetically modified viruses and our injection approach designed to avoid undue spread and non-specific potential contamination. We used

localized injection of Cre-dependent AAV virus (AAV8-hSyn-DIO-TC66T-2A-EGFP-2A-OG, 1.8×10^{12} genome units per mL) that expresses the avian viral receptor TVA, rabies G protein and EGFP to target CA3 subregions in the GAD-Cre mouse line. With the expression of TVA and G protein in the Cre+ neurons, we injected EnvA pseudotyped and glycoprotein gene-deleted (ΔG) rabies expressing DsRed (EnvA-SADΔG-RV-DsRed, 0.4 μL, approximately 2×10^7 infectious units per mL) into the same brain region of helper AAV injection at three weeks later. The EnvA pseudotyped rabies virus only infects the cells with the EnvA binding receptor, TVA expression, and this avoids the off-target expression in non-Cre or non-TVA cells (Wall *et al.*, 2010). After nine days of incubation that allows for for rabies virus in the EGFP and DsRed colocalized "starter neurons" to propagate retrogradely to their directly connected presynaptic neurons, the mice were perfused for tissue processing.

The helper AAV was delivered to the brain region of interest using iontophoretic current injection. This approach allows us to restrict the infected starter neurons in a small target region, like CA3a subregion, which we have verified as the sole injection and initial infection sites. Following visual check of the expression of the starter neurons labeled by both EGFP and mCherry in the whole hippocampal areas, cases with starter neurons that showed evidence for leak to adjacent brain regions were excluded from further analysis.

Rabies virus was locally made at the Center for Neural Circuit Mapping Center of the University of California, Irvine, with required cell lines and seeding viruses originally provided by E. Callaway's group at the Salk Institute for Biological Studies. The coordinates of dCA3 subregions relative to the bregma are anteroposterior (AP): −1.94mm, mediolateral (Rankov Petrovic *et al.*): −2.48 mm, dorsoventral (Lorincz *et al.*): −2.24 mm for CA3a, and AP: −2.06mm, ML: −1.92 mm, DV: −2.13 mm for CA3b/c (Fig 1 and S1 Table). All the mice were handled equally with receiving the same viral injections.

Histology and immunochemical staining

The mice were perfused with 5 mL of Phosphate Buffer Saline (PBS), followed by 25 mL PBS containing 4% paraformaldehyde. The perfused brains were removed, post-fixed in 4% paraformaldehyde overnight, then put into 30% sucrose in 1 X PBS for 24 hours. Dry ice was used to freeze the brain which was then coronally sectioned in 30-μm thickness on a freezing microtome (Leica SM2010R, Germany). Every one out of three sections was mounted for examination and quantification of virally labeled neurons in various brain structures and were then imaged for all subsequent computer-based analyses. Some brain sections were selected for neurochemical characterization of labeled cells.

To verify that starter neurons (which were selected based on the presence of EGFP and DsRed double-labeled cells in the dCA3 injection site) were inhibitory neurons, GABAergic immunostaining was performed. For GABA staining, a rabbit anti-GABA primary antibody (Sigma-Aldrich (St. Louis, MO, USA), A2052, 1:4000 dilution) was used followed by a Cy5-conjugated donkey anti-rabbit secondary antibody (Jackson ImmunoResearch (West Grove, PA, USA), 147088, 1:200 dilution). Furthermore, to investigate the subtypes of GABAergic inhibitory neurons in the injection site, brain sections (3 sections per case) were selected to immunostain for parvalbumin (PV), somatostatin (SOM), vasointestinal peptide

(VIP) and cholecystokinin (CCK). For PV staining, a rabbit anti-PV primary antibody (Aves Labs (Davis, CA, USA), PV27a_220208_500, 1:1000) was followed by the Cy5-conjugated donkey anti-rabbit secondary antibody. For SOM staining, a rat anti-SOM primary antibody (Novus Biology (Centennial, CO, USA), 158180, 1:500 dilution) was followed by a Cy5-conjugated donkey anti-rat secondary antibody (Jackson ImmunoResearch, 154628, 1:200 dilution). For VIP staining, a rabbit anti-VIP primary antibody (Immunostar (Hudson, WI, USA), 20077, 1:1000 dilution) was followed by the Cy5-conjugated donkey anti-rabbit secondary antibody. For CCK staining, a rabbit anti-CCK-8 primary antibody (Sigma (St. Louis, MO, USA), C-2581, 1:1000 dilution) was followed by the Cy5-conjugated donkey anti-rabbit secondary antibody. To enhance the expression of green fluorescent protein, all the sections were stained for GFP using a chicken anti-GFP primary antibody (Swant (Bellinzona, Switzerland), GFP3717982, 1:200 dilution) followed by an Alexa Fluor (AF) 488-conjugated donkey anti-chicken secondary antibody (Jackson ImmunoResearch (West Grove, PA, USA), 146581, 1:200 dilution). To delineate the hippocampal CA2 region, selected hippocampal sections were stained with a rabbit anti-PCP4 antibody (Invitrogen (Carlsbad, CA, USA), PA5-52209, 1:1000). This was followed by the Cy5-conjugated donkey anti-rabbit secondary antibody. Furthermore, sections from vCA1, SUBv, and SUBtr were selected for both inhibitory and excitatory immunostaining. To examine inhibitory cell labeling in these regions, the rabbit anti-GABA primary antibody followed by the Cy5-conjugated donkey anti-rabbit secondary antibody were used. To examine excitatory cell labeling, a mouse anti-CAMKIIα primary antibody (Thermo Fisher Scientific (Riverside, CA, USA), MA1-048, 1:1000 dilution) followed by the Cy5-conjugated donkey anti-mouse secondary antibody (Jackson ImmunoResearch (West Grove, PA, USA), 144119, 1:200). Details can be found in the S1b Table.

To acquire brain slice images of the mouse brain section series under a 10x objective, an automated slide scanning acquisition system (Metamorph, MDS Analytical Technologies, Sunnyvale, CA, USA) using a high-performance computer coupled with a fluorescent BX61 Olympus microscope and a high-sensitivity Hamamatsu CCD camera. Furthermore, labeled cells in selected sections were imaged with a confocal microscope (Fluoview 3000, Olympus Life Science Microscopy, Waltham, Massachusetts) coupled with z-stack and tile scanning features under a 20X objective. The confocal imaging system used dichroic mirrors for multicolor imaging. During 20x imaging for data acquisition by 640-nm excitation, the emission signal was acquired from 650 nm to 750 nm (pinhole: 1 AU). For data acquisition by 561 nm excitation, the emission was acquired from 570 nm to 614 nm (pinhole: 1 AU). For data acquisition by 488 nm excitation, the emission was acquired from 500 nm to 540 nm (pinhole: 1 AU). For data acquisition by 405 nm excitation, the emission was acquired from 430 nm to 470 nm (pinhole: 1 AU). The image stack (~30 μm per brain section; step size: 2 μm) was acquired by the Fluoview 3000 software using the OIR file format, then converted to a maximal projection image in a TIFF format which was later used during cell counting. Quantitative examinations of virally labeled neurons across the series of brain sections were conducted for complete and unbiased analyses using Adobe Photoshop software (Adobe Systems, San Jose, California, USA).

Data quantification

Regarding the counting protocol, brain sections with the target injection regions (either dCA3a or dCA3b/c), were selected to identify GFP and DsRed double-labeled starter neurons. Starter neurons were manually measured using the counting tool in Photoshop. To correctly identify CA3 subdomains, Thompson et. al's mapping of CA3 boundaries was used (Thompson *et al.*, 2008). Franklin and Paxinos' mouse brain atlas images (Franklin KBJ) were aligned to the rest of the brain sections and used to determine accurate anatomical structures for the quantification of remaining DsRed labeled cells. No stereological protocol was used; all labeled cells in each section of the brain section series (i.e., 1 out of every 3 sections was mounted for examination of virally labeled neurons in different brain structures) were counted.

We calculated the connection strength index (CSI), defined as the ratio of the number of presynaptic neurons in a brain region of interest versus the number of postsynaptic (starter) neurons in CA3. We also calculated the proportion of inputs (PI) defined as the ratio of the number of presynaptic inputs versus the number of total inputs. These values were utilized to quantitatively compare the inputs to CA3 inhibitory and excitatory neurons along the proximodistal and septotemporal axes (S2 Table). The raw counting data is shown in Table S4. To assure objectivity of our analysis, histological processing and neuronal counting were conducted in a double-blind procedure.

Statistics

Data were presented as mean ± SD, or mean ± SE. For statistical comparison between two groups that were not normally distributed, a non-parametric-unpaired t-test (Mann-Whitney U Test) was used. This is in line with routine guidelines for a relatively small sample size and does not require assumptions of normality or equal variance required for parametric tests. Alpha levels of $p \leq 0.05$ were considered significant. For statistical comparisons across more than 2 groups, the nonparametric version of 1-way ANOVA (Kruskal–Wallis test) was first used, and if the outcome was significant, Dunn's multiple comparison tests were conducted between groups with multiple comparison corrections as needed. Statistical data is shown in Table S3.

Results

Monosynaptic rabies viral tracing of synaptic inputs to inhibitory neurons in dorsal CA3 subregions

We mapped brain-wide circuit inputs to hippocampal CA3 inhibitory neurons using monosynaptic retrograde rabies virus-mediated tracing. To specifically target inhibitory neurons in dCA3, we used GAD2-Cre mice (Taniguchi *et al.*, 2011) for Cre-dependent rabies virus tracing that selectively targets inhibitory neurons in dCA3 subregions along the proximodistal (transverse) axis (Fig 1A). As rabies virus labeling has the feature of measurable starter cells at the injection site, connectivity strengths of input mapped brain regions per starter cell can be measured quantitatively. We calculated the connection strength index (CSI), defined as the ratio of the number of presynaptic neurons in a brain region of interest versus the number of postsynaptic (starter) neurons in CA3.

In our approach, the rabies virus targets specific cell types using EnvA pseudotyping; glycoprotein transcomplementation restricts transsynaptic propagation to the presynaptic cells that provide direct inputs to starter neurons (Sun *et al.*, 2014; Wall *et al.*, 2010; Wickersham *et al.*, 2007). The EnvA receptor TVA expression in starter cells allows EnvA pseudotyped, G-deleted rabies virus to enter the starter cells. The TVA is an avian receptor protein that is absent in mammalian cells unless it is expressed through exogenous gene delivery. The rabies glycoprotein (RG) and TVA are genetically delivered by the helper AAV to neurons in the specific injection sites, such as dCA3 for the present case, but not other brain regions in a Cre mouse line. Following the helper injection, the EnvA-pseudotyped ΔG rabies virus enters Cre+ cells that express the TVA receptor. Because the Cre+ cells express rabies glycoprotein, the EnvA-pseudotyped ΔG rabies virus can complete trans-complementation and then spreads retrogradely to label direct presynaptic neurons.

We virally traced circuit connections to a small population of dCA3 starter cells located in different dCA3 subregions (average number of starters per case: dCA3a, 26 ± 5 neurons, n = 8 mice; dCA3b/c, 19 ± 5 neurons, n = 6 mice) (S2 Table). Note that the injection location at distal dCA3 is termed dCA3a (corresponding to domain # 3, based on the updated criteria defined by Thompson and colleagues (Thompson *et al.*, 2008). The relatively proximal location of dCA3 is termed dCA3b/c (corresponding to domains # 2 and 1). Distal and proximal dCA3 are separated by the midline of fimbria.

The starter cells can be unambiguously identified by their EGFP and DsRed expression (Fig 1B and 1C). We stained the hippocampal sections with GABA antibody to verify that the labeled starter neurons are inhibitory interneurons. Our staining result shows that 97.1% of starter neurons (n = 6 mice) in the dCA3 injection site are immunopositive for GABA thus confirming they are inhibitory neurons (Fig 1D and H).

We further examined the subtypes of the inhibitory neurons in dCA3 injection regions. The hippocampal sections containing starter neurons were stained with antibodies for somatostatin (SOM), parvalbumin (PV), vasoactive intestinal peptide (VIP) and cholecystokinin (CCK) (Fig 1E–G and S2 Fig). The distribution of GABAergic subtype inhibitory neurons in dCA3 that we observe is consistent with previous literature (Freund and Buzsaki, 1996). More than half of dCA3 GABAergic inhibitory neurons are SOM+ (64.3%), followed by PV+ and VIP + with 33.59% and 14.22%, respectively (3 hippocampal sections per case, SOM, n = 8 cases; PV, n = 6 cases; VIP, n = 6 cases) (Fig 1H). The colocalization of starter neurons and CCK-expressing inhibitory neurons (n = 3 cases) is observed in dCA3 subregions (S2 Fig).

Brain-wide canonical inputs to inhibitory neurons in dCA3

Following rabies-mediated viral injection, the presynaptic neurons that provide inputs to dCA3 subregions, express DsRed in input brain regions including the medial septum and diagonal band of Broca (MS-DBB), dentate gyrus (DG), CA2, entorhinal cortex (EC), retromammillary (RM) nucleus, and the median raphe nucleus (MnR) (Fig 2A–I). These input brain regions have been previously identified as connected to dCA3, therefore they are designated as canonical inputs. Quantitative comparisons of presynaptic input strengths along the proximodistal axis are shown in Fig 2J and K (S2 and S3 Tables) by using the

input connection strength index (CSI). We also calculated the proportion of inputs (PI) index by dividing the total labeled neurons in all of the input brain regions by the number of labeled presynaptic neurons in the brain region of interest (Fig 2K, S2 and S3 Tables) to determine the relative input distribution for a given target region. MS-DBB and DG have stronger input connections to proximal dCA3 (CA3b/c) than the distal dCA3 (dCA3a) (Figure 2A–B, E–F). Our results show that MS-DBB is the primary long-range input of dCA3 subregions (CSI: dCA3a = 4.62 ± 0.27, n = 8 mice; dCA3b = 6.12 ± 0.60, n = 6 mice; Mann-Whitney U test, $p = 0.022$) (Fig 2J, S2 and S3 Tables). On average, the granular layer of DG (GrDG) and hilus provide approximately 2-fold stronger inputs to proximal dCA3 as compared to distal dCA3 (CSI for GrDG: dCA3a = 0.91 ± 0.26, n = 8 mice; dCA3b/c = 2.12 ± 0.61, n = 6 mice; Mann-Whitney U test, $p = 0.073$; CSI for DG-hilus: dCA3a = 0.37 ± 0.14, n = 8 mice; dCA3b = 1.34 ± 0.43, n = 6 mice; Mann-Whitney U test, $p = 0.055$) (Fig 2B, 2F, 2J and S2 and S3 Tables). The p values have a significant trend. CA2 provides relatively strong hippocampal input to dCA3 (Fig 2I and 2J). Purkinje cell protein 4 (PCP4) immunostaining was used to delineate the CA2 region (Fig 2I) (San Antonio et al., 2014). The mossy fiber tract as well as the cytoarchitectural feature of the pyramidal layer identified by the DAPI staining allows us to distinguish CA2 from distal dCA3 and the proximal CA1 region. No CSI differences are observed between CA3a/b and CA3 subregions in other input regions, including CA2, EC, MnR and RM. Additionally, sparse inputs are observed in the medial entorhinal cortex (Monte Domecq) and lateral entorhinal cortex (LEC) (Fig 2C and 2G). MEC and LEC input labels are restricted to layer II. Labeled neurons are also found in RM and MnR (Fig 2D and 2H). No significant differences are observed in the PI measurements of canonical inputs between dCA3a and dCA3b/c (Fig 2K). Detailed quantification data can be found in Supplementary Tables 2 and 3.

Differential ipsilateral and contralateral CA3 inputs to CA3 inhibitory and excitatory neurons

To study local CA3 circuit input connections, we compare the inputs to inhibitory and excitatory neurons in dCA3 subregions along the proximodistal and septotemporal axes. The hippocampus has traditionally been subdivided based on neuronal architecture (Ramón, 1911). More recently, the hippocampus has been anatomically parsed further by transcriptomic expression data. Following Thompson's genomic study (Thompson *et al.*, 2008), dCA3 input regions are split into 3 subdomains (domain 1 (D1), domain 2 (D2), and domain 3 (D3) that correspond to dCA3c, dCA3b, and dCA3a, respectively) along proximodistal (transverse) axis. Ventral CA3 (vCA3) is divided into 6 subdomains along the septotemporal (longitudinal) axis, but rabies-virus labeled neurons in the current study are limited to domain 4 (D4) and domain 5 (D5). We first mapped the ipsilateral inputs to dCA3 inhibitory neurons in proximal and distal dCA3 subregions (Fig 3A). Both proximal and distal dCA3 subregions receive substantial inputs from more distal portions of dCA3 (D3). The input connection strength gradually reduces along a distal to proximal gradient (CSI for D1: dCA3a = 3.64 ± 0.61, dCA3b/c = 5.63 ± 1.10; CSI for D2: dCA3a = 11.32 ± 1.64, dCA3b/c = 22.49 ± 3.88; CSI for D3: dCA3a = 25.84 ± 2.34, dCA3b/c = 29.17 ± 3.53. $n = 8$ mice for dCA3a, $n = 6$ mice for dCA3b/c) (Fig 3E and S2 Table). For CA3 subdomains D1, D2, D3, D4 and D5, the connectivity of septotemporal inputs is not as strong as the inputs at the transverse level (Kruskal-Wallis (KW) test results for D1, D2, D3, D4 and D5 are p

= 0.0067, p = 0.0466, p = 0.0903, p = 0.0133 and p = 0.0366, respectively). The majority of ventral CA3 input neurons are located at D4 and are restricted within the ventral DG (CSI for D4: CA3a = 0.95 ± 0.13, CA3b/c = 1.71 ± 0.51; CSI for D5: CA3a = 6.97 ± 0.85, CA3b/c = 6.12 ± 1.33. n = 8 mice for CA3a, n = 6 mice for CA3b/c) (Fig 3A and 3E). No significant difference of CSI is observed with the injection regions of inhibitory neurons located in distal or proximal regions (Fig 3E). In contrast to the strong ipsilateral inputs measured, the contralateral CA3 subregions have sparse connections with dCA3 inhibitory neurons (Fig 3B). Despite their weak connectivity, the contralateral inputs follow the same pattern as the ipsilateral inputs. Distally positioned contralateral CA3 neurons tend to have slightly stronger inputs to CA3 inhibitory neurons (CSI for contra D1: dCA3a = 0.22 ± 0.09, dCA3b/c = 0.23 ± 0.20; CSI for contra D2: dCA3a = 0.76 ± 0.26, dCA3b/c = 1.10 ± 0.20; CSI for contra D3: dCA3a = 1.93 ± 0.42, dCA3b/c = 1.83 ± 0.21; CSI for contra D4: dCA3a = 0.19 ± 0.09, dCA3b/c = 0.22 ± 0.13; CSI for contra D5: dCA3a = 1.33 ± 0.59, dCA3b/c = 0.71 ± 0.34. KW test results for contra D1, D2, D3, D4, and D5 are p = 0.0023, p = 0.0060, p = 0.0242, p = 0.0348 and p = 0.0300, respectively. n = 8 mice for CA3a, n = 6 mice for CA3b/c) (Fig 3E and S2–3 Tables).

Extending beyond the connection patterns of CA3-to-CA3 inhibitory neurons, we also examined the CA3 inputs to excitatory neurons in dCA3 subregions. To label the excitatory neurons, we injected the helper AAV and rabies virus into dCA3 subregions in Camk2a-Cre mice (n = 4 for dCA3a, n = 4 for dCA3b/c) (S1A–C Fig) (Tsien *et al.*, 1996). We find differences in connectivity of excitatory neurons compared to inhibitory neurons in CA3; distal CA3 neurons have the strongest inputs to CA3 excitatory neurons in distal subregions but not in proximal subregions. The 3 subdomains along the axis give rise to similar levels of input strength to proximally located excitatory neurons (CA3 excitatory neurons tracing results, CSI for D1: dCA3a = 10.29 ± 1.41, dCA3b/c = 8.56 ± 1.35; CSI for D2: dCA3a = 19.97 ± 2.58, dCA3b/c = 13.74 ± 3.02; CSI for D3: dCA3a = 34.36 ± 7.48, dCA3b/c = 16.49 ± 3.63) (Fig 3C and 3E). The KW test results for D1, D2 and D3 are p = 0.0067, p = 0.0466 and p = 0.0903, respectively (S3 Table). Dunn comparison tests for D1, GAD-Cre CA3a vs. CAMK2a-Cre CA3a indicate a significant difference, p = 0.0137 (S3 Table).

The local inputs to the proximal CA3 excitatory neurons are restricted to the transverse level, but the distal CA3 receives extensive inputs throughout subregions along the septotemporal axis (Fig 3C). The distally positioned excitatory neurons have 12-fold higher connection strength with ventral CA3 relative to proximally positioned dCA3 neurons (CSI for D4: dCA3a = 6.13 ± 2.24, dCA3b/c = 0.54 ± 0.41; CSI for D5: dCA3a = 7.38 ± 3.07, dCA3b/c = 0.791 ± 0.40. KW test results for D4 and D5 are p = 0.0133 and p = 0.0366, respectively. Dunn's comparison test for D4: CA3a vs.CA3b/c, p = 0.0195) (Fig 3E and S3 Table). With respect to contralateral connections, the excitatory neurons show significantly higher CSI values compared to CA3 inhibitory neurons (CSI for contra D1: dCA3a = 2.49 ± 0.79, dCA3b/c = 1.21 ± 0.33; CSI for contra D2: dCA3a = 6.99 ± 2.45, dCA3b/c = 2.08 ± 0.98; CSI for contra D3: dCA3a = 8.98 ± 2.55, dCA3b/c = 2.82 ± 0.87; CSI for contra D4: dCA3a = 3.59 ± 2.08, dCA3b/c = 0.15 ± 0.11; CSI for contra D5: dCA3a = 3.25 ± 2.07, dCA3b/c = 0.10 ± 0.05. KW test results for contra D1, D2, D3, D4, and D5 are p = 0.0023, p = 0.0060, p = 0.0242, p = 0.0348 and p = 0.0300, respectively.) (Fig 3D and 3E). vCA3 neurons show strong inputs to the excitatory neurons in distal dCA3

relative to proximal neurons (GAD-Cre CA3a vs. Camk2a-Cre CA3a: Dunn's comparison test for contra D4, $p = 0.0466$) (Fig 3 and S3 Table). As shown in the CSI values, the PI measurements of CA3-to-CA3 local connections indicate similar patterns between the subregions and neuronal subtypes (S1 Fig, S2 and S3 Tables)

Noncanonical inputs from dorsal and ventral CA1 to dCA3 inhibitory neurons

Using the rabies viral tracing approach, we also find substantial noncanonical inputs to CA3 inhibitory neurons from CA1 subregions along the septotemporal axis that have not been characterized earlier (Fig 4). In relation to our previous findings for excitatory neurons (Lin *et al.*, 2021), CA1 is split into dorsal CA1 (dCA1), dorsal-ventral CA1 (vCA1d), intermediate-ventral (vCA1i), and ventral-ventral (vCA1v) subdivisions based on the spatial expression of specific gene markers (Dong *et al.*, 2009). The border between vCA1d and vCA1i is delineated by the ventral edge of the DG lateral blade, and the border of vCA1i and vCA1v is at the same level as the dorsal edge of the rhinal fissure. We find that CA3 inhibitory neurons receive inputs from both dCA1 and vCA1 (anterior-posterior (AP) distance from Bregma: −1.94 mm to −3.52 mm) (Fig 4A). The dCA1 input neurons extend to pyramidal and oriens layers (Fig 4B). Immunostaining results confirm the identity of these input cells as inhibitory neurons as they are GABA-positive and immuno-negative for the excitatory cell marker calmodulin-dependent protein kinase II alpha (CaMKIIα) (Fig 4C). Note that presynaptic inputs in vCA1 are spatially located at the top and intermediate portions of vCA1 (vCA1d and vCA1i). The majority of inputs are observed in the superficial pyramidal layer with more densely packed DAPI staining indicating higher cellular density (Fig 4D–G). All the input neurons are immunostained as GABA- and CaMKIIα+ in the triple label composite (Fig 4H).

To assess whether CA1 inputs to dCA3 inhibitory neurons follow a topographic pattern as we find with excitatory neurons in CA3 (Lin *et al.*, 2021), we compare CSI and PI measurements to CA3 subregions along the transverse axis. We do not find that dCA1 projections innervate differentially to inhibitory neurons in dCA3 subregions (CSI for dCA1: dCA3a = 1.17 ± 0.63, n = 8 mice; dCA3b/c = 0.38 ± 0.18, n = 6 mice; Mann-Whitney U test, $p = 0.571$) (Fig 4B, 4I, S2 and S3 Tables). The CSI measurements show that vCA1 excitatory neurons in the pyramidal layer (vCA1 py.) have significantly stronger connections with the inhibitory neurons located in the proximal dCA3 (dCA3a) as compared to the neurons close to the distal dCA3 (dCA3b/c) (CSI for vCA1 py.: dCA3a = 2.08 ± 0.51, n = 8 mice; dCA3b/c = 0.49 ± 0.14, n = 6 mice; Mann-Whitney U test, $p = 0.003$) (Fig 4I, S2 and S3 Tables). The somata of excitatory vCA1 neurons located close to the oriens layer follow a similar trend seen with vCA1py neurons (CSI for vCA1 or.: dCA3a = 0.67 ± 0.15, n = 8 mice; dCA3b/c = 0.25 ± 0.05, n = 6 mice; Mann-Whitney U test, $p = 0.008$) (Fig 4I, S2 and S3 Tables). The PI measurements of CA1 subregions are significantly different between CA3a and CA3b/c (PI for dCA1: dCA3a = 0.018 ± 0.011, dCA3b/c = 0.004 ± 0.002; PI for vCA1py.: dCA3a = 0.032 ± 0.009, dCA3b/c = 0.007 ± 0.003; PI for vCA1 or.: dCA3a = 0.009 ± 0.002, dCA3b/c = 0.003 ± 0.001. Mann-Whitney U test results are $p = 0.280$, $p = 0.008$, and $p = 0.008$ for dCA1, vCA1 py. and vCA1 or., respectively. n = 8 mice for dCA3a and n = 6 mice for dCA3b/c) (Fig 4J, S2 and S3 Tables).

Noncanonical inputs from subiculum complex to dCA3 subregions.

CA3 excitatory neurons receive relatively weak inputs from the ventral subiculum (SUBv) and subiculum transition zone (SUBtr) subregions (Fig 5). Further details concerning the anatomical delineation of the subiculum complex can be found in recent anatomical mapping and tracing studies (Ding *et al.*, 2020; Lin *et al.*, 2021). We differentiate subiculum complex into the "classical" dorsal subiculum as SUBdd (aka dSUB or SUB), the intermediate portion of the ventral subiculum as SUBv, and the tip of the ventral subiculum as SUBvv in accordance with prior definitions (Fig 5A). The SUBtr is close to the presubiculum (PrS), parasubiculum (PaS), and MEC (Fig 5E). Many rabies-labeled presynaptic neurons are spatially located at the top and intermediate portions of SUBv (close to the SUBdd region) (Fig 5B). Compared to the inhibitory neurons located at proximal dCA3, the more distally positioned CA3 neurons have stronger connections with the SUBv region (CSI for SUBv: dCA3a = 0.45 ± 0.12, n = 8 mice; dCA3b/c = 0.04 ± 0.02, n = 6 mice, Mann-Whitney U test, $p = 0.0047$) (Fig 5B, 5C, 5I, S2 and S3 Tables). We also observe that sparse presynaptic SUBtr neurons located at the top and intermediate portions have similar levels of input strength to dCA3 subregions (CSI for SUBtr: dCA3a = 0.07 ± 0.02, n = 8 mice; dCA3b/c = 0.09 ± 0.07, n = 6 mice, Mann-Whitney U test, $p = 0.375$) (Fig 5F, 5G, 5I, S2 and S3 Tables). The immunostaining results reveal that the rabies-mediated viral labeled presynaptic inputs in SUBv and SUBtr regions are excitatory neurons as they are negative for GABA and positive for CaMKIIα immunostaining (Fig 5D and 5H). As shown in the CSI values, the PI measurements of SUBtr indicate a similar topographic gradient pattern to CA3 subregions (Fig 5J, S2 and S3 Tables).

Discussion

We have mapped brain-wide circuit inputs to inhibitory neurons in dCA3 using retrograde monosynaptic rabies viral tracing. We find substantial back projection from the CA1 and the subiculum complex to dCA3 that run in the opposite direction of the feedforward trisynaptic pathway, and opposite the septotemporal axis. The input strengths of the noncanonical circuits vary according to the dCA3 locations along the transverse axis.

Using GAD-Cre transgenic mice to target GABAergic inhibitory neurons is an effective means for studying all inputs for these neurons. Inhibitory neurons only account for 10–15% of the neurons in the hippocampus, but these relatively small numbers belie their complexity: there are at least 13 types of inhibitory neurons in the hippocampus (Freund and Buzsaki, 1996; Pelkey *et al.*, 2017). Hippocampal inhibitory neurons are diverse in anatomical, morphological and physiological connections, and they exhibit overlapping characteristics as well (Freund and Buzsaki, 1996). Therefore, it is difficult to find a single defined subtype of inhibitory neurons based on the additional complexity conferred by gene markers. The relatively low number of inhibitory neurons presents a technical challenge, but this can be addressed. To study CA3 sub-regional anatomical connections, we used the ionotropic approach to restrict the retrograde rabies virus to a small group of neurons in targeted CA3 subregions. We used GAD-Cre mice to label all subtypes of inhibitory neurons. The starter inhibitory neurons are spatially restricted to the CA3 oriens and pyramidal layers.

Rabies viral tracing allows us to quantitatively analyze CA3 input connections at a cell-type-specific level. This is enabled by the expression of helper AAV and rabies virus in a measurable group of defined starter neurons that allows us to assess the connection strengths of the brain regions / sub-regions that provide inputs. Using this approach, we confirmed CA3 input strengths to dCA3 inhibitory and excitatory neurons follow a gradient pattern along the CA3 transverse axis (Fig 6A–B). This is generally consistent with previous anatomical tracing results (Amaral and Witter, 1989; Ishizuka *et al.*, 1990; Li *et al.*, 1994).

Major brain regions that provide typical inputs to CA3 inhibitory neurons include the medial septum, the dentate gyrus, the entorhinal cortex and CA3. By comparing the input connection patterns and strengths to inhibitory neurons to excitatory neurons in dCA3, we find that their distributions of inputs are differentially organized between ventral and contralateral CA3 subregions (Fig 6A–B and Fig S1). The ventral CA3 inputs are connected to inhibitory neurons in proximal and distal dCA3 subregions. In contrast, excitatory neurons in dCA3 receive long-distance inputs from more temporal regions (like D4), while the vCA3 inputs to inhibitory neurons in dCA3 originate from a more septal subregion (D5), and project relatively shorter distances to dCA3.

The major difference for contralateral CA3 subregions is that inputs from contralateral CA3 vary by the neuronal type and CA3 sub-region (Fig 6A–B). Several studies have shown that CA3a (distal) have homotopic connections with contralateral CA3 subregions (Andersen *et al.*, 1969; Blackstad, 1956; Voneida *et al.*, 1981), but prior to this study, little was known about the inputs to the CA3c (proximal) regions as well as the differences between the inputs to the excitatory and inhibitory neurons (Laurberg, 1979; Voneida *et al.*, 1981; West *et al.*, 1979). Our data show that contralateral inputs to excitatory neurons in dCA3 follow a similar gradient pattern to those seen for associational inputs from ipsilateral dCA3, which receive the most robust inputs from distal dCA3 (CA3a), and gradually decrease along the distal-proximal axis. We observe sparse contralateral connections to CA3 inhibitory neurons, compared to the input strengths to excitatory neurons.

The relative strengths of canonical inputs to CA3 inhibitory neurons differ in three brain regions, this result is consistent with our findings described in our CA3 excitatory neuron tracing study (Lin *et al.*, 2021). First, the medial septal has a 1.6-fold stronger connection with the dCA3 inhibitory neurons compared to the excitatory neurons. Proximally located excitatory and inhibitory neurons in dCA3 receive relatively stronger inputs from MS. In contrast to the MS, the dentate gyrus and the entorhinal cortex display relatively 5-fold stronger connections with excitatory neurons compared to inhibitory neurons in dCA3. The DG inputs to dCA3 exhibit a topographical gradient with CSI values that decrease from proximal to distal subregions. No such topological differences are observed in the inputs from EC to dCA3.

Our data support the existence of extensive, noncanonical circuitry projecting to CA3 inhibitory neurons in the hippocampal formation. We mapped the noncanonical inputs from vCA1 and SUB complex to both excitatory and inhibitory neurons in dCA3; the back-projections run in the opposite direction of the canonical feedforward trisynaptic pathway (Lin *et al.*, 2021). Noncanonical inputs from vCA1 and subicular complex to CA3 inhibitory

neurons follow a proximodistal topographic gradient with regard to CA3 subregions (Fig 6C). We find novel noncanonical circuit connections between inhibitory CA3 neurons and vCA1, subiculum complex and other brain regions. Note that the overall connection strength of the vCA1 inputs is similar to that of mossy-fiber inputs. The results support the idea that noncanonical inputs may complement and augment the trisynaptic pathway within the hippocampal formation.

Supplementary Material

Refer to Web version on PubMed Central for supplementary material.

Acknowledgments:

This work was supported by NIH BRAIN Initiative grants [NS078434 (X.X.). MH120020 (X.X.)]. T.C.H. is supported by NIH R35 GM127102. We thank Yihan Wang for providing help with making schematic illustrations. The authors declare no competing interests.

Statement of data availability

The data that supports the findings of this study are available in the supplementary material of this article.

References

Acsady L, Kamondi A, Sik A, Freund T and Buzsaki G (1998). GABAergic cells are the major postsynaptic targets of mossy fibers in the rat hippocampus. J Neurosci, 18, 3386–3403. [PubMed: 9547246]

Amaral DG and Witter MP (1989). The three-dimensional organization of the hippocampal formation: a review of anatomical data. Neuroscience, 31, 571–591. [PubMed: 2687721]

Andersen P, Bliss TV, Lomo T, Olsen LI and Skrede KK (1969). Lamellar organization of hippocampal excitatory pathways. Acta Physiol Scand, 76, 4A–5A.

Andersen P, Bliss TV and Skrede KK (1971). Lamellar organization of hippocampal pathways. Exp Brain Res, 13, 222–238. [PubMed: 5570425]

Blackstad TW (1956). Commissural connections of the hippocampal region in the rat, with special reference to their mode of termination. J Comp Neurol, 105, 417–537. [PubMed: 13385382]

Cenquizca LA and Swanson LW (2007). Spatial organization of direct hippocampal field CA1 axonal projections to the rest of the cerebral cortex. Brain Res Rev, 56, 1–26. [PubMed: 17559940]

Chamberland S and Topolnik L (2012). Inhibitory control of hippocampal inhibitory neurons. Front Neurosci, 6, 165. [PubMed: 23162426]

Ding SL, Yao Z, Hirokawa KE, Nguyen TN, Graybuck LT, Fong O, Bohn P, Ngo K, Smith KA, Koch C, Phillips JW, Lein ES, Harris JA, Tasic B and Zeng H (2020). Distinct Transcriptomic Cell Types and Neural Circuits of the Subiculum and Prosubiculum along the Dorsal-Ventral Axis. Cell Rep, 31, 107648. [PubMed: 32433957]

Dong HW, Swanson LW, Chen L, Fanselow MS and Toga AW (2009). Genomic-anatomic evidence for distinct functional domains in hippocampal field CA1. Proc Natl Acad Sci U S A, 106, 11794–11799. [PubMed: 19561297]

Franklin KBJ PG Paxinos and Franklin's The mouse brain in stereotaxic coordinates. 4th ed, 1 volume (unpaged)

Freund TF and Antal M (1988). GABA-containing neurons in the septum control inhibitory interneurons in the hippocampus. Nature, 336, 170–173. [PubMed: 3185735]

Freund TF and Buzsaki G (1996). Interneurons of the hippocampus. Hippocampus, 6, 347–470. [PubMed: 8915675]

Germroth P, Schwerdtfeger WK and Buhl EH (1989). GABAergic neurons in the entorhinal cortex project to the hippocampus. Brain Res, 494, 187–192. [PubMed: 2765919]

Ishizuka N (2008). [Longitudinal fiber systems in the hippocampal formation]. Brain Nerve, 60, 737–745. [PubMed: 18646613]

Ishizuka N, Weber J and Amaral DG (1990). Organization of intrahippocampal projections originating from CA3 pyramidal cells in the rat. J Comp Neurol, 295, 580–623. [PubMed: 2358523]

Jackson J, Amilhon B, Goutagny R, Bott JB, Manseau F, Kortleven C, Bressler SL and Williams S (2014). Reversal of theta rhythm flow through intact hippocampal circuits. Nat Neurosci, 17, 1362–1370. [PubMed: 25174002]

Jaffe DB and Gutierrez R (2007). Mossy fiber synaptic transmission: communication from the dentate gyrus to area CA3. Prog Brain Res, 163, 109–132. [PubMed: 17765714]

Joshi A, Salib M, Viney TJ, Dupret D and Somogyi P (2017). Behavior-Dependent Activity and Synaptic Organization of Septo-hippocampal GABAergic Neurons Selectively Targeting the Hippocampal CA3 Area. Neuron, 96, 1342–1357 e1345. [PubMed: 29198757]

Klausberger T and Somogyi P (2008). Neuronal diversity and temporal dynamics: the unity of hippocampal circuit operations. Science, 321, 53–57. [PubMed: 18599766]

Knierim JJ and Neunuebel JP (2016). Tracking the flow of hippocampal computation: Pattern separation, pattern completion, and attractor dynamics. Neurobiol Learn Mem, 129, 38–49. [PubMed: 26514299]

Korol DL, Abel TW, Church LT, Barnes CA and McNaughton BL (1993). Hippocampal synaptic enhancement and spatial learning in the Morris swim task. Hippocampus, 3, 127–132. [PubMed: 8353599]

Laurberg S (1979). Commissural and intrinsic connections of the rat hippocampus. J Comp Neurol, 184, 685–708. [PubMed: 422759]

Lawrence JJ and McBain CJ (2003). Interneuron diversity series: containing the detonation--feedforward inhibition in the CA3 hippocampus. Trends in Neurosciences, 26, 631–640. [PubMed: 14585604]

Lee H, Wang C, Deshmukh SS and Knierim JJ (2015). Neural Population Evidence of Functional Heterogeneity along the CA3 Transverse Axis: Pattern Completion versus Pattern Separation. Neuron, 87, 1093–1105. [PubMed: 26298276]

Lee I, Yoganarasimha D, Rao G and Knierim JJ (2004). Comparison of population coherence of place cells in hippocampal subfields CA1 and CA3. Nature, 430, 456–459. [PubMed: 15229614]

Leutgeb S, Leutgeb JK, Treves A, Moser MB and Moser EI (2004). Distinct ensemble codes in hippocampal areas CA3 and CA1. Science, 305, 1295–1298. [PubMed: 15272123]

Li XG, Somogyi P, Ylinen A and Buzsaki G (1994). The hippocampal CA3 network: an in vivo intracellular labeling study. J Comp Neurol, 339, 181–208. [PubMed: 8300905]

Lin X, Amalraj M, Blanton C, Avila B, Holmes TC, Nitz DA and Xu X (2021). Noncanonical projections to the hippocampal CA3 regulate spatial learning and memory by modulating the feedforward hippocampal trisynaptic pathway. PLOS Biology, 19, e3001127. [PubMed: 34928938]

Lorincz T, Kisfali M, Lendvai B and Sylvester Vizi E (2016). Phenotype-dependent Ca(2+) dynamics in single boutons of various anatomically identified GABAergic interneurons in the rat hippocampus. Eur J Neurosci, 43, 536–547. [PubMed: 26566266]

Lu L, Igarashi KM, Witter MP, Moser EI and Moser MB (2015). Topography of Place Maps along the CA3-to-CA2 Axis of the Hippocampus. Neuron, 87, 1078–1092. [PubMed: 26298277]

Marr D (1971). Simple memory: a theory for archicortex. Philos Trans R Soc Lond B Biol Sci, 262, 23–81. [PubMed: 4399412]

Melzer S, Michael M, Caputi A, Eliava M, Fuchs EC, Whittington MA and Monyer H (2012). Long-range-projecting GABAergic neurons modulate inhibition in hippocampus and entorhinal cortex. Science, 335, 1506–1510. [PubMed: 22442486]

Misgeld U and Frotscher M (1986). Postsynaptic-GABAergic inhibition of non-pyramidal neurons in the guinea-pig hippocampus. Neuroscience, 19, 193–206. [PubMed: 3537840]

Monte Domecq R. n. (1911). La república del Paraguay en su primer centenario, 1811–1911. Compañía sud-americana de billetes de banco, Buenos Aires,, pp. 2 p. l., 3 –472 p., 471 l., viii p. incl. illus., ports.

Pelkey KA, Chittajallu R, Craig MT, Tricoire L, Wester JC and McBain CJ (2017). Hippocampal GABAergic Inhibitory Interneurons. Physiol Rev, 97, 1619–1747. [PubMed: 28954853]

Picard C, Fieschi C, Altare F, Al-Jumaah S, Al-Hajjar S, Feinberg J, Dupuis S, Soudais C, Al-Mohsen IZ, Genin E, Lammas D, Kumararatne DS, Leclerc T, Rafii A, Frayha H, Murugasu B, Wah LB, Sinniah R, Loubser M, Okamoto E, Al-Ghonaium A, Tufenkeji H, Abel L and Casanova JL (2002). Inherited interleukin-12 deficiency: IL12B genotype and clinical phenotype of 13 patients from six kindreds. Am J Hum Genet, 70, 336–348. [PubMed: 11753820]

Ramón Y, Cajal S (1911). Histologie du Systeme Nerveux de l'Homme et des Vertebres. Maloine, Paris.

Rankov Petrovic B, Hrncic D, Mladenovic D, Simic T, Suvakov S, Jovanovic D, Puskas N, Zaletel I, Velimirovic M, Cirkovic V, Macut D, Stanojlovic O and Rasic-Markovic A (2019). Prenatal Androgenization Induces Anxiety-Like Behavior in Female Rats, Associated with Reduction of Inhibitory Interneurons and Increased BDNF in Hippocampus and Cortex. Biomed Res Int, 2019, 3426092. [PubMed: 31281833]

Salib M, Joshi A, Katona L, Howarth M, Micklem BR, Somogyi P and Viney TJ (2019). GABAergic Medial Septal Neurons with Low-Rhythmic Firing Innervating the Dentate Gyrus and Hippocampal Area CA3. J Neurosci, 39, 4527–4549. [PubMed: 30926750]

Scoville WB and Milner B (1957). Loss of recent memory after bilateral hippocampal lesions. J Neurol Neurosurg Psychiatry, 20, 11–21. [PubMed: 13406589]

Steward O (1976). Topographic organization of the projections from the entorhinal area to the hippocampal formation of the rat. J Comp Neurol, 167, 285–314. [PubMed: 1270625]

Sun Y, Jin S, Lin X, Chen L, Qiao X, Jiang L, Zhou P, Johnston KG, Golshani P, Nie Q, Holmes TC, Nitz DA and Xu X (2019). CA1-projecting subiculum neurons facilitate object-place learning. Nat Neurosci, 22, 1857–1870. [PubMed: 31548723]

Sun Y, Nguyen AQ, Nguyen JP, Le L, Saur D, Choi J, Callaway EM and Xu X (2014). Cell-type-specific circuit connectivity of hippocampal CA1 revealed through Cre-dependent rabies tracing. Cell Rep, 7, 269–280. [PubMed: 24656815]

Sun Y, Nitz DA, Holmes TC and Xu X (2018). Opposing and Complementary Topographic Connectivity Gradients Revealed by Quantitative Analysis of Canonical and Noncanonical Hippocampal CA1 Inputs. eNeuro, 5.

Swanson LW and Cowan WM (1977). An autoradiographic study of the organization of the efferent connections of the hippocampal formation in the rat. J Comp Neurol, 172, 49–84. [PubMed: 65364]

Swanson LW, Sawchenko PE and Cowan WM (1981). Evidence for collateral projections by neurons in Ammon's horn, the dentate gyrus, and the subiculum: a multiple retrograde labeling study in the rat. J Neurosci, 1, 548–559. [PubMed: 6180146]

Taniguchi H, He M, Wu P, Kim S, Paik R, Sugino K, Kvitsiani D, Fu Y, Lu J, Lin Y, Miyoshi G, Shima Y, Fishell G, Nelson SB and Huang ZJ (2011). A resource of Cre driver lines for genetic targeting of GABAergic neurons in cerebral cortex. Neuron, 71, 995–1013. [PubMed: 21943598]

Thompson CL, Pathak SD, Jeromin A, Ng LL, MacPherson CR, Mortrud MT, Cusick A, Riley ZL, Sunkin SM, Bernard A, Puchalski RB, Gage FH, Jones AR, Bajic VB, Hawrylycz MJ and Lein ES (2008). Genomic anatomy of the hippocampus. Neuron, 60, 1010–1021. [PubMed: 19109908]

Tsien JZ, Chen DF, Gerber D, Tom C, Mercer EH, Anderson DJ, Mayford M, Kandel ER and Tonegawa S (1996). Subregion- and cell type-restricted gene knockout in mouse brain. Cell, 87, 1317–1326. [PubMed: 8980237]

Voneida TJ, Vardaris RM, Fish SE and Reiheld CT (1981). The origin of the hippocampal commissure in the rat. Anat Rec, 201, 91–103. [PubMed: 7030147]

Wall NR, Wickersham IR, Cetin A, De La Parra M and Callaway EM (2010). Monosynaptic circuit tracing in vivo through Cre-dependent targeting and complementation of modified rabies virus. Proc Natl Acad Sci U S A, 107, 21848–21853. [PubMed: 21115815]

West JR, Nornes HO, Barnes CL and Bronfenbrenner M (1979). The cells of origin of the commissural afferents to the area dentata in the mouse. Brain Res, 160, 203–215. [PubMed: 83896]

Wickersham IR, Lyon DC, Barnard RJ, Mori T, Finke S, Conzelmann KK, Young JA and Callaway EM (2007). Monosynaptic restriction of transsynaptic tracing from single, genetically targeted neurons. Neuron, 53, 639–647. [PubMed: 17329205]

Witter MP (2007). Intrinsic and extrinsic wiring of CA3: indications for connectional heterogeneity. Learn Mem, 14, 705–713. [PubMed: 18007015]

Witter MP, Doan TP, Jacobsen B, Nilssen ES and Ohara S (2017). Architecture of the Entorhinal Cortex A Review of Entorhinal Anatomy in Rodents with Some Comparative Notes. Front Syst Neurosci, 11, 46. [PubMed: 28701931]

Wittner L, Henze DA, Zaborszky L and Buzsaki G (2006). Hippocampal CA3 pyramidal cells selectively innervate aspiny interneurons. Eur J Neurosci, 24, 1286–1298. [PubMed: 16987216]

Xu X, Sun Y, Holmes TC and Lopez AJ (2016). Noncanonical connections between the subiculum and hippocampal CA1. J Comp Neurol, 524, 3666–3673. [PubMed: 27150503]

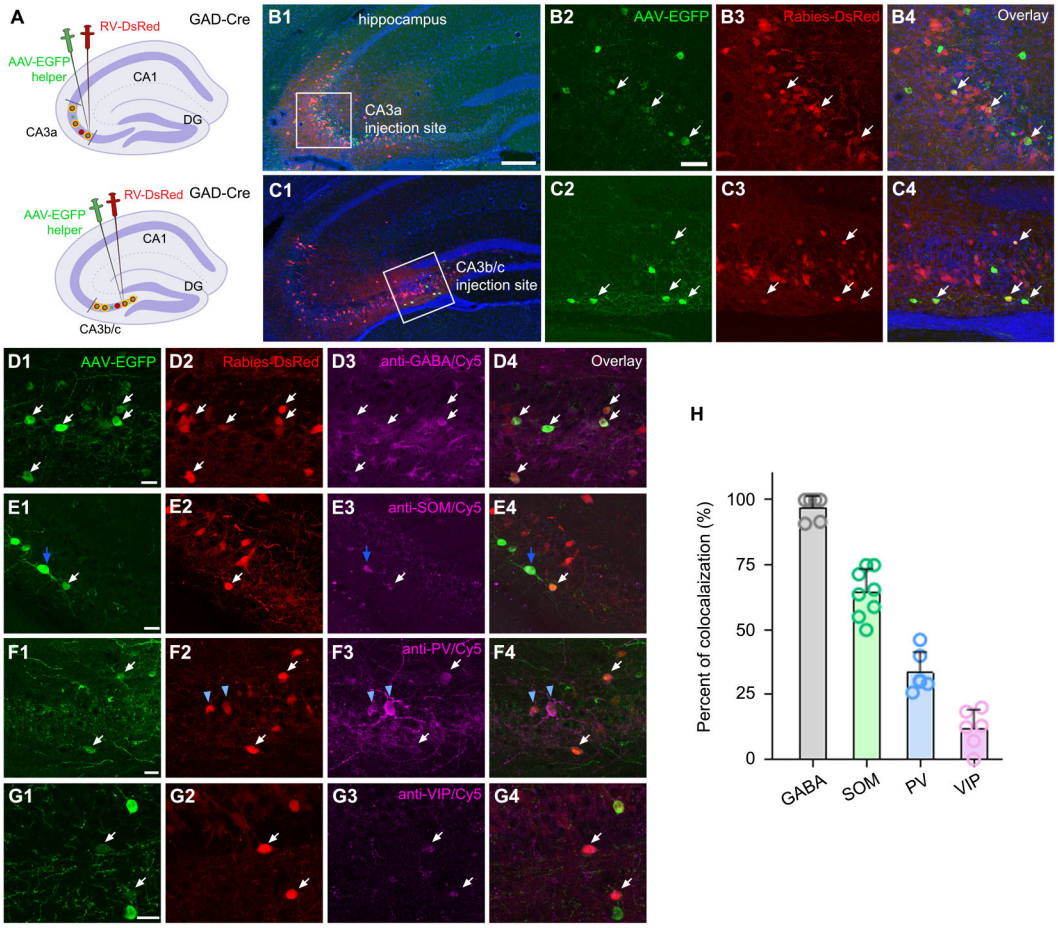

Fig 1: Immunochemical characterization of hippocampal CA3 inhibitory neurons targeted by Cre-dependent monosynaptic rabies tracing in GAD-Cre mice.

(A) Schematic of monosynaptic retrograde rabies virus (RV) tracing genetically targeted to inhibitory neurons in dorsal CA3 (dCA3) subregions. Cre-dependent AAV-EGFP helper virus (AAV8-hSyn-DIO-TC66T-2A-eGFP-2A-OG, green) is injected into specific dCA3 subregions of GAD-Cre mice, followed by injection of the rabies virus (RV-DsRed: EnvA-SADΔG-RV-DsRed, red) in the same locations 3 weeks later. From top to bottom, CA3a and CA3b/c injection schematics are shown. **(B–C)** Coronal sections of injection sites in two CA3 subregions (**B1-B4** for CA3a, **C1-C4** for CA3b/c). Injection sites are shown in white boxes along the proximodistal (transverse) axis. The insets of the white box regions are shown for CA3a (**B2-B4**) and CA3b/c (**C2-C4**). Images in **B2** and **C2** show EGFP-labeled inhibitory cells (green). Images in **B3** and **C3** allow for visualization of rabies labeled neurons by DsRed. Images in **B4** and **C4** show EGFP and DsRed double-labeled starter neurons (white arrows). The scale bar (200 μm) applies to **B1** and **C1**. The scale bar (50 μm) applies to **B2-B4** and **C2-C4**. **(D)** Immunostaining and confocal images depict GABAergic starter neurons in the dCA3 injection site. The EGFP expression of the AAV-helper virus is enhanced by an AF488-conjugated secondary antibody (**D1**). Rabies-virus-infected neurons are labeled by DsRed (**D2**). GABAergic immunoreactivity is revealed with a Cy5-conjugated secondary antibody shown in pink pseudo-color (**D3**). The white arrows in each panel for **D** indicate GABAergic immunostained starter neurons. **(E-G)** Example images of

inhibitory interneuron subtypes in dCA3 injection site (the same format as in **D**). The white arrow indicates that the starter neuron is immunopositive for either somatostatin (SOM), parvalbumin (PV), or vasoactive intestinal peptide (VIP) in the dCA3 injection site. The blue arrow points to an AAV-EGFP helper infected cell that is SOM+ (**E1-E4**). The light blue arrowhead reveals the rabies-infected presynaptic neurons in PV-expressing inhibitory neurons in CA3 (**F2-F4**). The scale bar (20 μm) applies to all the panels. **(H)** Quantification of starter neurons as calculated by the immunochemically identified subtypes of inhibitory neurons in dCA3. n = 8 mice (3 hippocampal sections per mice) for SOM, and n = 6 mice for GABA, PV, and VIP immunostaining. Data are represented as mean ± SE.

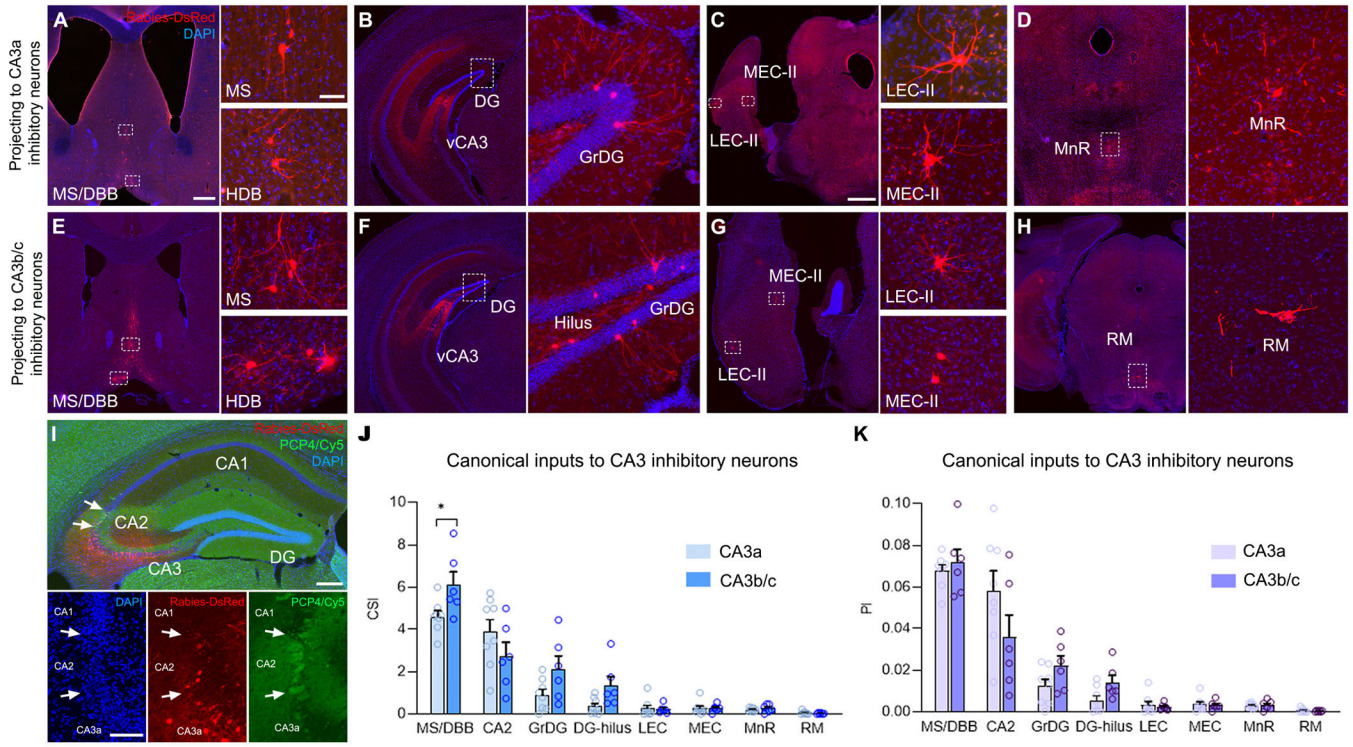

Fig 2. Canonical brain region inputs to inhibitory neurons in CA3a and CA3b/c subregions verified by Cre-dependent monosynaptic RV tracing.

(A-D) Representative images showing monosynaptic RV labeled neurons that project to CA3a in presynaptic input regions. Presynaptic cells are found in the MS, the HDB of Broca (**A**), the GrDG (**B**), the LEC and MEC (**C**), and the MnR (**D**). **(E-H)** are formatted similarly to **A-D** to illustrate canonical inputs to the CA3b/c inhibitory neurons from MS/DBB, GrDG, EC, RM, and MnR. **(I)** The example images show presynaptic inputs from CA2. The arrows indicate the border of CA1, CA2 and CA3 determined by DAPI and PCP4 staining. **(J)** Quantitative measurements of input connection strengths by the connection strength index (CSI) following rabies tracing from CA3a and CA3b/c subregions. The data were measured from 14 GAD-Cre mice with n = 8 mice for CA3a and n = 6 mice for CA3b/c subregions. All data are presented as mean ± SE. *, indicates the CSI statistical significance level of $p \leq 0.05$ (Mann-Whitney U test). **(K)** Measurements of proportion of inputs (PI) for specific brain regions following rabies tracing from CA3a and CA3b/c subregions. The raw data are included in the S2–4 tables. The scale bar (800 μm) applies to left panels in **C** and **H**. The scale bar (400 μm) applies to left panels in **A, B, D, E, F** and **G**. The scale bar (200 μm) applies to **I**. The scale bar (100 μm) applies to all of the enlarged panels from **A** to **I**. GrDG, granule layer of the dentate gyrus; HDB, horizontal diagonal band; LEC-II, layer II of lateral entorhinal cortex; MEC-II, layer II of medial entorhinal cortex; MnR, median raphe nucleus; MS medial septum; RM, retromammillary; vCA3, ventral CA3; VDB, vertical diagonal band.

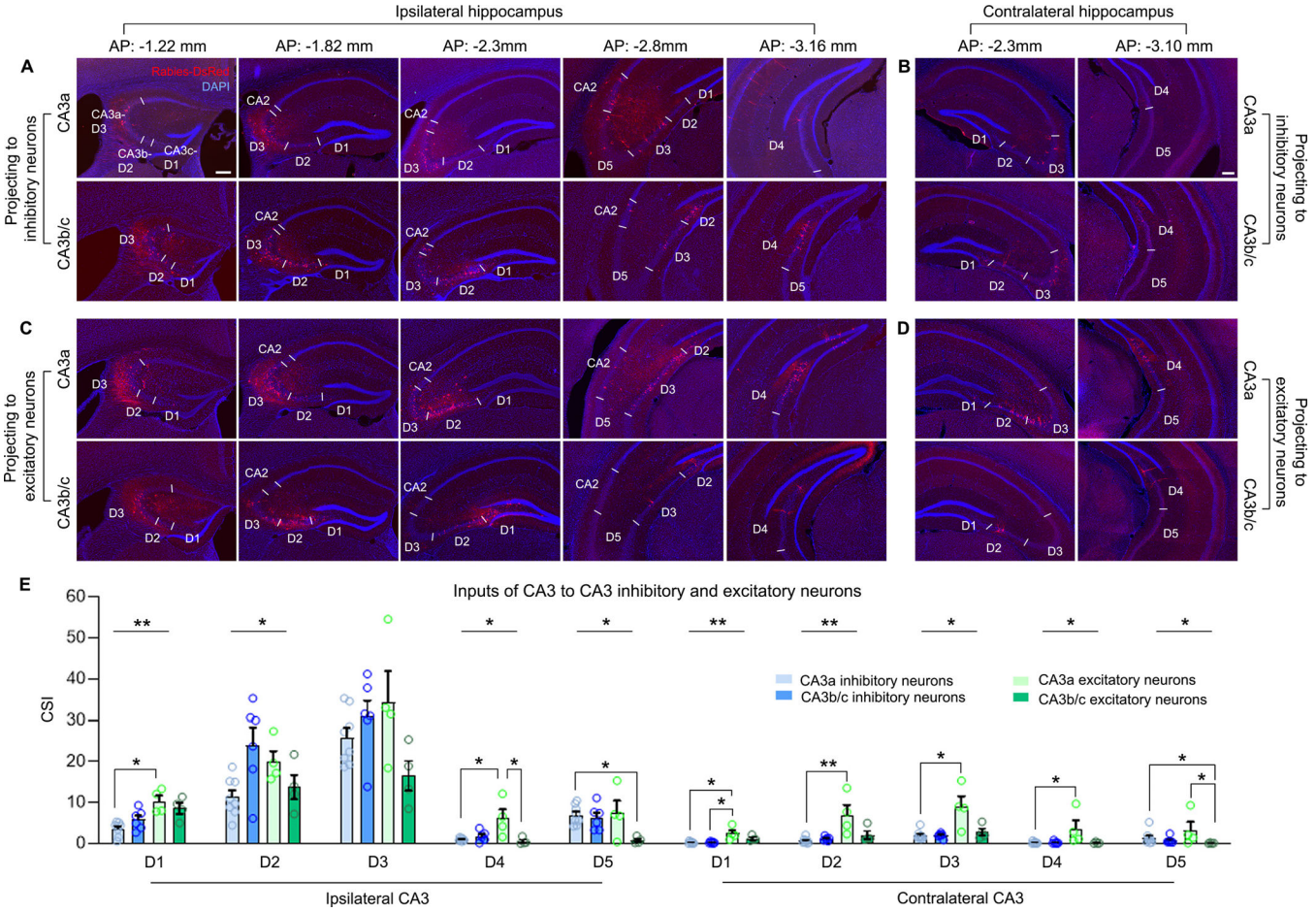

Fig 3. Local circuit input connections to inhibitory and excitatory neurons within CA3a and CA3b/c subregions show differential dorsal/ventral gradients and ipsilateral/contralateral input strengths.

(**A–B**) Representative images show the distribution of ipsilateral and contralateral CA3 inputs to the inhibitory neurons in CA3a and CA3b/c subregions using GAD-Cre mice. - The expression of presynaptic RV is visualized with DsRed in red, DAPI staining is blue. The AP number indicates the distance from the coronal section (30- μm thick) to the bregma. The white lines delineate the 5 subdomains of CA3 and CA2. The dCA3 includes D1, D2, D3 corresponding to CA3c, CA3b, and CA3a, respectively. The ventral CA3 includes D4 and D5. (**C-D**) are formatted similarly to **A-B** which shows presynaptic RV input cells from ipsilateral and contralateral CA3 subregions to CA3 excitatory neurons in the CA3a and CA3b/c subregions. The scale bar (200 μm) applies to all the panels. (**E**) Quantitative results depict input connection strengths to CA3 inhibitory neurons and excitatory neurons measured by the CSI across CA3 subdomains along proximodistal and septotemporal axes following RV tracing in CA3 subregions. Data for inhibitory neurons are from 14 GAD-Cre mice (n = 8 mice for CA3a and n = 6 for CA3b/c region). Data for excitatory neurons are from 8 Camk2a-Cre mice (n = 4 mice for CA3a and n = 4 for CA3b/c region). All data are presented as mean ± SE; *, **, indicates the CSI statistical significance level of $p \leq 0.05$ and $p \leq 0.01$ (Kruskal–Wallis test followed by Dunn's comparison test). The results of the Kruskal–Wallis tests are indicated by the upper horizontal lines comparing different cell

groups and subregions, and the results of Dunn's tests are indicated by the brackets above the bars between different cell groups and subregions. The raw data for E and F are included in S2–S4 tables.

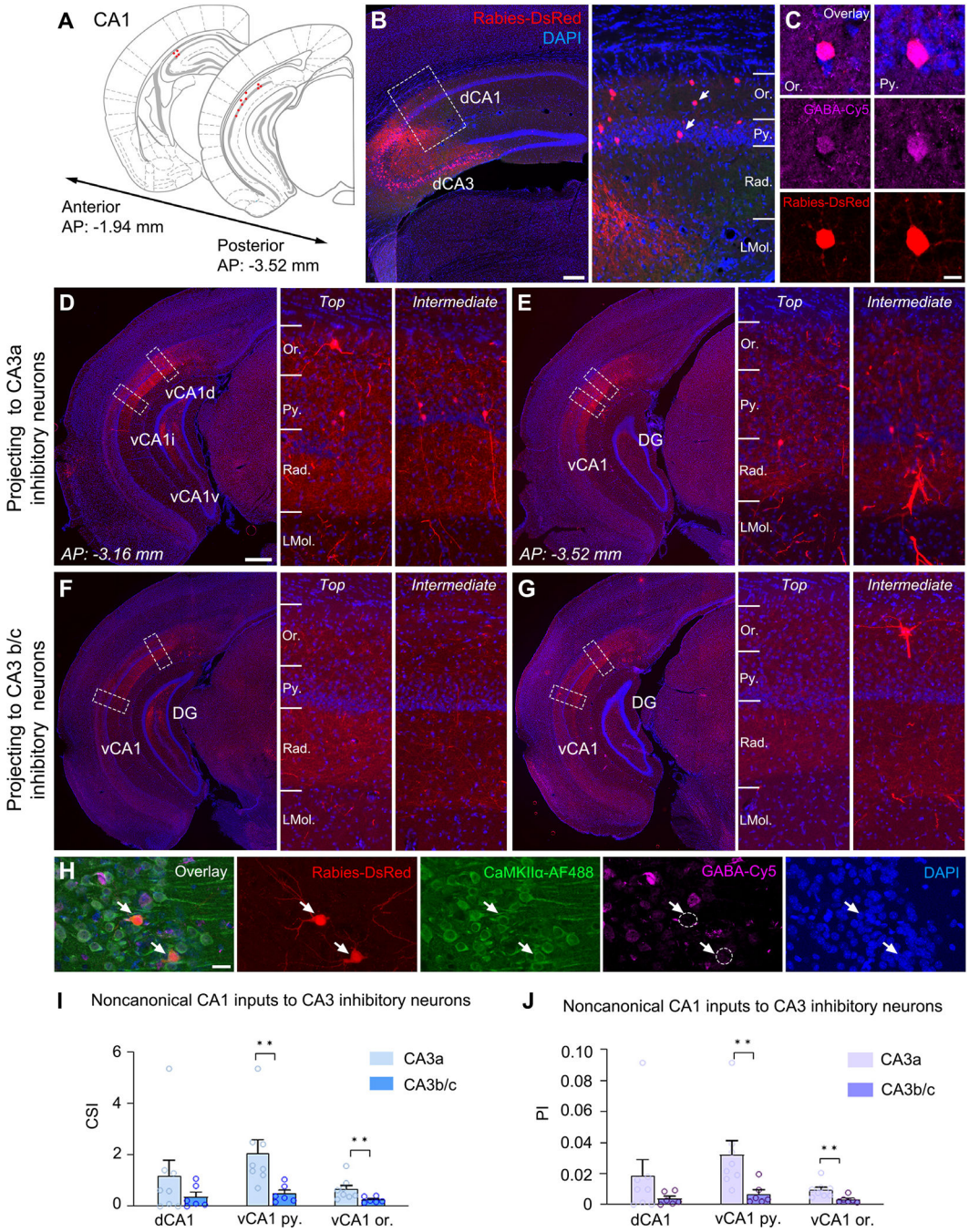

Fig 4. Noncanonical inputs from CA1 to inhibitory neurons in CA3a and CA3b/c subregions show distinct topographic input strength gradients that decrease along distal/proximal axes.

(A) Schematics illustrate the RV tracing results of dCA3 subregions and the noncanonical input regions, including dorsal CA1 (dCA1) and ventral CA1 (vCA1) along the septotemporal axis. Retrogradely labeled neurons are depicted in red with a large pseudo-size for visualization. The AP coordinates from the Bregma are provided. (**B**) Representative images show dCA1 inputs with enlarged views shown on the right oriented from top to bottom. White arrowheads point to the input neurons. (**C**) Representative images of

GABA immunostained RV-labeled presynaptic neurons in dCA1. A small region of interest in the overlay image (**B**) is enlarged to single cell resolution in **C**. RV-labeled neurons are visualized by DsRed expression. GABAergic immunoreactivity is visualized with a Cy5-conjugated secondary antibody depicted as pink pseudo-color, DAPI is blue. (**D-E**) Representative coronal sections showing the expression of presynaptic inputs from vCA1 to CA3a along the septotemporal axis. The boxed regions at vCA1 in the left panels are shown in the middle and right panels at a higher magnification. The vCA1 inputs are located at oriens (or.) and pyramidal (py.) layers. **(F-G)** are formatted similarly to D-E to illustrate noncanonical vCA1 inputs to CA3b/c subregion. **(H)** Representative images of CaMKIIα and GABA immunostained RV-labeled presynaptic neurons in vCA1. RV-labeled neurons are visualized by DsRed expression. CaMKIIα immunoreactivity is visualized with a AF488 conjugated secondary antibody in green pseudo-color. GABAergic immunoreactivity is visualized with an Cy5-conjugated secondary antibody as pink. White arrows indicate the colocalization of RV-labeled neurons and CaMKIIα+ immunostaining neurons. Dash circle delineates an RV-labeled neuron as GABA-negative. The scale bar (500 μm) applies to left panels in **D**, **E**, **F** and **G**. The scale bar (200 μm) applies to the left panel in **B**. The scale bar (50 μm) applies to all the magnified input regions from **B** to **G**. The scale bar (50 μm) applies to **H**. The scale bar (10 μm) applies to **C**. **(I)** Quantitative analyses of input connection strengths measured by the CSI across dCA1 and vCA1 following RV tracing in CA3 subregions. vCA1 inputs are organized by the spatial location at the pyramidal layer (vCA1 py.) and oriens layer (vCA1 or.). n = 8 mice for CA3a and n = 6 for CA3b/c region. Data are from 14 GAD-Cre mice. All data are presented as mean ± SE; ** indicates the CSI statistical significance level of $p \leq 0.01$ (Mann-Whitney U test). See S3 table for more statistical information. **(J)** Quantitative measurements of the PI for specific brain regions following the same format as in **I**. The raw data for **I** and **J** are included in S4 table.
CSI, connection strength index; dCA1, dorsal CA1; DG, dentate gyrus; LMol., lacunosum moleculare layer; or., oriens layer; PI, proportion index; py., pyramidal layer; rad., radiatum layer; vCA1, ventral CA1; vCA1d, dorsal part of ventral CA1; vCA1i, intermediate part of ventral CA1; vCA1v, ventral part of ventral CA1.

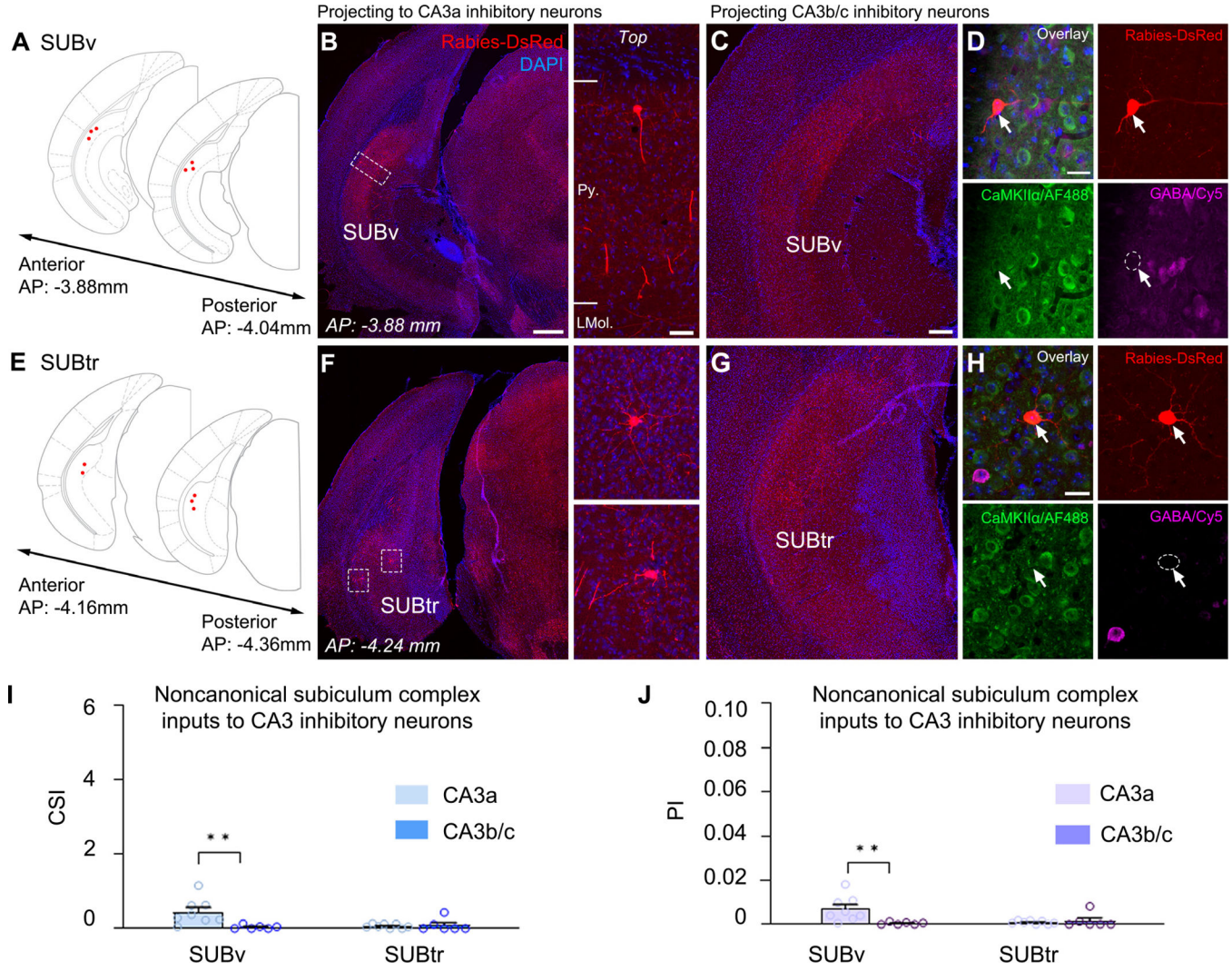

Fig 5. Noncanonical inputs from SUBv and SUBtr to inhibitory neurons are sparse but show quantitatively greater inputs to CA3a than CA3b/c subregions.

(A) Schematic figures show the RV tracing results of dCA3 subregions and the noncanonical inputs from SUBv along the septotemporal axis. Retrogradely labeled neurons are depicted in red with a large pseudo-size for visualization. The AP coordinates from the Bregma are provided. (**B-C**) Representative images show the inputs from SUBv to CA3a and CA3b/c subregions. The region within the white rectangle on the left side of **B** is depicted on the right side of **B** to show single cell resolution of the inputs. (**D**) Representative images of CaMKIIα and GABA immunostained RV-labeled presynaptic neurons in SUBv. RV-labeled neurons labeled by DsRed expression are depicted as red. CaMKIIα immunoreactivity is visualized with a AF488 conjugated secondary antibody are shown in green pseudo-color. GABAergic immunoreactivity visualized by an Cy5-conjugated secondary antibody are depicted as pink. White arrows indicate the colocalization of dual labeled RV-labeled neuron that express CaMKIIα+ excitatory neurons. The dashed circle delineates an RV-labeled excitatory neuron as GABA-negative. (**E-H**) are formatted similarly to **A-D** to illustrate noncanonical inputs to CA3a and CA3b/c subregions from SUBtr. The scale bar (500 μm)

applies to left panels in **B** and **F**. The scale bar (200 μm) applies to left panels in **C** and **G**. The scale bar (50 μm) applies to all the magnified input regions in **B**, **C**, **F** and **G**. The scale bar (20 μm) applies to **D** and **H**. **(I)** Quantitative analyses of input connection strengths measured by the CSI across SUBv and SUBtr following RV tracing in CA3 subregions. n = 8 mice for CA3a and n = 6 for CA3b/c region. Data are from 14 GAD-Cre mice. All data are presented as mean ± SE; **, indicates the CSI statistical significance level of $p \leq 0.01$, respectively (Mann-Whitney U test). See S3 table for p values for other brain regions. **(J)** Quantitative measurements of the PI for specific brain regions following the same format as in **I**. The raw data for **I** and **J** are included in S4 table. CSI, connection strength index; LMol., lacunosum moleculare layer; PI, proportion index; py., pyramidal layer; SUBtr, subiculum transition area; SUBv, ventral subiculum.

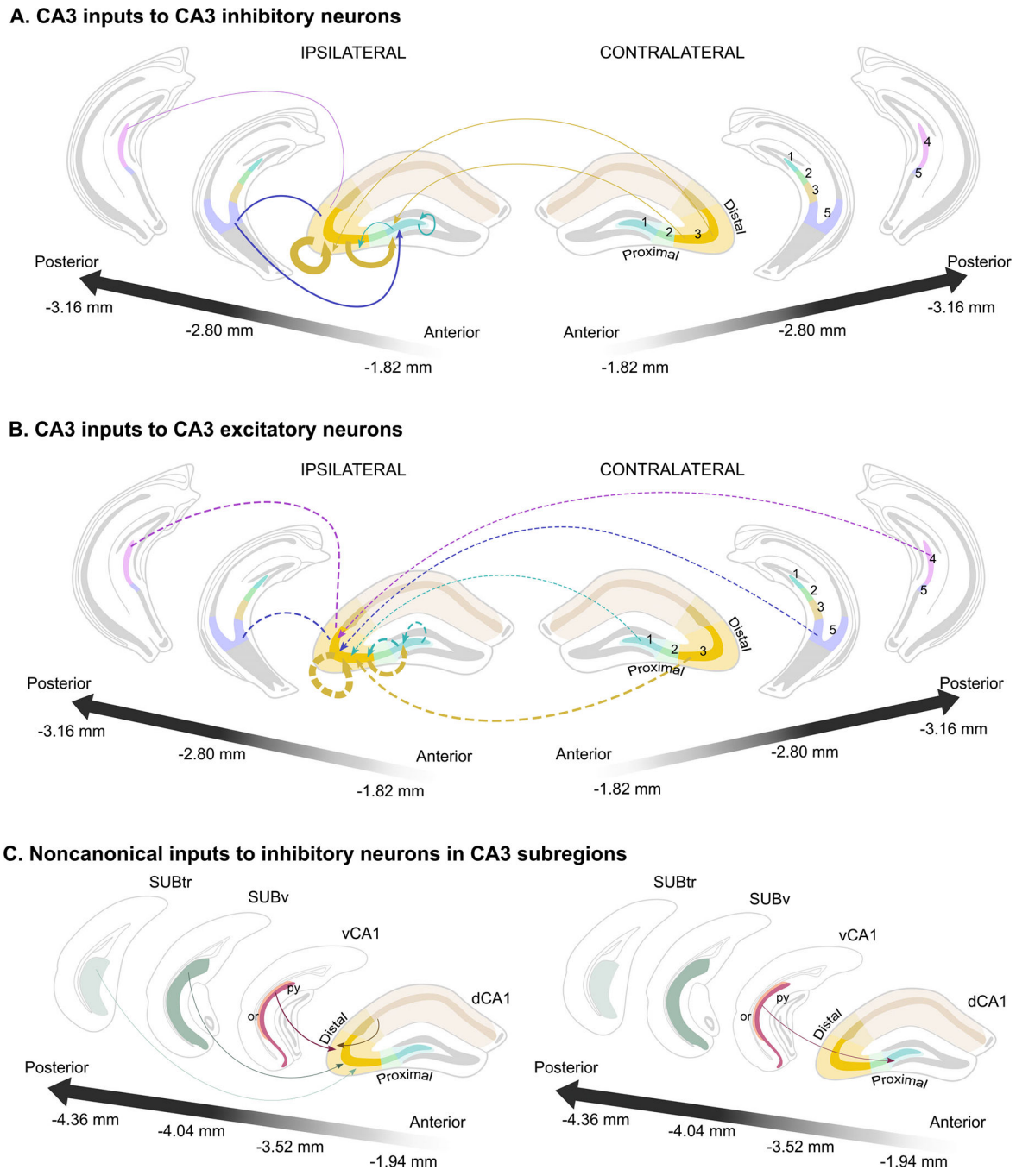

Fig 6. Schematic summary of hippocampal local circuitry and the noncanonical inputs to dCA3 subregions.

(A) The summary diagram of CA3 inputs to the inhibitory neurons in dCA3 subregions. The input CA3 subregions, D1, D2, D3, D4 and D5 are organized from the proximodistal and septotemporal axes. Colors represent the subregions of each CA3 input region. The projection direction is indicated by a color-labeled arrow from the corresponding input regions, and the thickness of the arrow indicates the connectivity strength. **(B)** The diagram is formatted similarly to A to depict the CA3 inputs to the excitatory neurons in dCA3

subregions. **(C)** The summary diagram of spatial topology of noncanonical inputs to distal and proximal regions of dCA3 (CA3a and CA3b/c). The input regions dCA1, vCA1, SUBv and SUBtr are organized from the septal to temporal direction. Shades of the same color indicate different layers in each input region. dCA1, dorsal CA1; dCA3, dorsal CA3; or, oriens layer; py, pyramidal layer; SUBtr, subiculum transition area; SUBv, ventral subiculum; vCA1, ventral CA1.